Early Structural Evolution of Native Cytochrome c after Solvent Removal

Michal Z. Steinberg,[d] Ron Elber,[b] Fred W. McLafferty,[c] R. Benny Gerber,[d] and Kathrin Breuker*[a]

Electrospray ionization transfers thermally labile biomolecules, such as proteins, from solution into the gas phase, where they can be studied by mass spectrometry. Covalent bonds are generally preserved during and after the phase transition, but it is less clear to what extent noncovalent interactions are affected by the new gaseous environment. Here, we present atomic-level computational data on the structural rearrangement of native cytochrome c immediately after solvent removal. The first structural changes after desolvation occur surprisingly early, on a timescale of picoseconds. For the time segment of up to 4.2 ns investigated here, we observed no significant breaking of native noncovalent bonds; instead, we found formation of new noncovalent bonds. This generally involves charged residues on the protein surface, resulting in transiently stabilized intermediate structures with a global fold that is essentially the same as that in solution. Comparison with data from native electron capture dissociation experiments corroborates both its mechanistic postulations and our computational predictions, and suggests that global structural changes take place on a millisecond timescale not covered by our simulations.

Introduction

The structural study of biomolecules by mass spectrometry (MS) has recently emerged as a promising alternative to conventional condensed-phase methods, such as nuclear magnetic resonance (NMR) spectroscopy and X-ray crystallography. There is evidence that aspects of native protein[1] and nucleic acid[2] structure can be retained after solvent removal in electrospray ionization (ESI)[3] MS experiments. However, atomic-level detail for biomolecular structures in the gas phase is not yet available. Here, we report computational data on the structural changes of native protein structure immediately after desolvation. As a model system we chose equine (Fe^{III})–cytochrome c, because it is well characterized in solution and has also been studied in gas-phase experiments.[4] Equine cytochrome c is a 104 residue electron-transfer protein with a covalently bound heme group; in solution, all charged residues are surface exposed, with the charges pointing away from the protein surface for efficient solvation in water (Figure 1).[5]

ESI produces gas phase ions directly from solution, and accumulating evidence suggests that the charge residue model (CRM)[6] is the dominating process during ESI of native proteins.[7] It is assumed that solvent evaporation from nanometer-sized droplets that contain only one protein ion each results in the formation of gaseous ions. We have recently studied this desolvation process by molecular dynamics (MD) simulations, and observed no appreciable changes in the native (Fe^{III})–cytochrome c structure during water evaporation.[8] Moreover, we found that the last water molecules to evaporate aggregate around charged sites, and thereby shield any intramolecular charge–charge and charge–dipole interactions in the largely desolvated structure. Here, we report MD simulations of equine (Fe^{III})–cytochrome c in the complete absence of solvent, with focus on the very first structural changes caused by dehydration. For evaluation of computational results, we
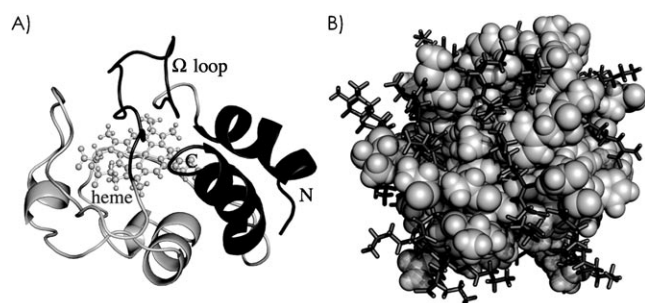
Figure 1. NMR structure (PDB ID: 1AKK)[5] of native equine (Fe^{III})–cytochrome c. A) N-terminal helix (residues 1–13), C-terminal helix (89–104), and Ω loop (18–34) are shown in dark gray; B) charged residues are shown in dark gray.

[a] Dr. K. Breuker
Institute of Organic Chemistry
and Center for Molecular Biosciences Innsbruck (CMBI)
University of Innsbruck, Innrain 52a, 6020 Innsbruck (Austria)
Fax: (+43) 512-507-2892
E-mail: kathrin.breuker@uibk.ac.at

[b] Prof. R. Elber
Department of Chemistry and Biochemistry
Institute of Computational Engineering
University of Texas, Austin, TX 78712 (USA)

[c] Prof. F. W. McLafferty
Department of Chemistry and Chemical Biology
Cornell University, Ithaca, NY 14853-1301 (USA)

[d] M. Z. Steinberg, Prof. R. B. Gerber
Department of Physical Chemistry, Fritz Haber Research Center
Hebrew University, Jerusalem 91904 (Israel)

compare the MD data with experimental data from native electron capture dissociation (NECD)[9] experiments.

Results and Discussion

### Reorientation of charged side chains

Visual inspection of the protein structures from relatively short (0–20 ps) and highly resolved MD simulations showed that the first structural rearrangements after desolvation generally involve charged side chains. Most of these were found to rapidly collapse onto the protein surface, as illustrated for protonated K79 forming an ionic hydrogen bond (iHB) with the amide oxygen of Y48 (Figure 2).
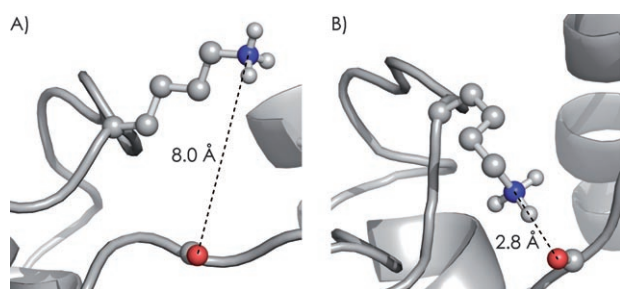
Figure 2. Rapid formation of an ionic hydrogen bond, shown here for protonated K79 and amide oxygen of Y48. A) NMR structure 1AKK. B) Molecular Dynamics snapshot after 15 ps simulation time.

Attractive interactions of charged residues in proteins include charge–charge (salt bridge, SB) and charge–dipole (iHB) interactions. We therefore analyzed our MD data for the number of salt bridges and ionic hydrogen bonds that involved positively ((+)iHB) as well as negatively ((−)iHB) charged side chains. Figure 3 shows that the number of SBs increased from six in the solution structure to an average value of 17.3 within the first 10 ps. Within the same time span, the number of (+)- and (−)iHBs increased from zero to 11.6 on average, and from five to 6.3, respectively. The number of positively and negatively charged side chains in native cytochrome c at pH 5 is 21 and 12, respectively;[10] this means that some of the charged side chains participate in more than one electrostatic interaction.

The average number of electrostatic interactions increased exponentially with simulation time, with rate constants of $(1.497 \pm 0.020) \times 10^{12}$, $(0.533 \pm 0.004) \times 10^{12}$, and $(0.523 \pm 0.012) \times 10^{12}$ s^{-1} for SB, (+)-, and (−)iHB formation, respectively. Plateau values from the exponential fits were 17.2, 11.7, and 6.1 for SB, (+)- and (−)iHB formation, respectively, which is very close to the above average values for 10 ps simulation time. Considering the error limits, the rate constants for (+)- and (−)iHB formation were the same, whereas SB formation proceeded about 2.8-times faster. This finding is consistent with the long-range potential of charge–charge interactions ($1/r$ distance dependence), and the shorter-range potential of charge–dipole interactions ($1/r^2$ or $1/r^4$ distance dependence, depending on whether the dipole is fixed or freely rotating).[11]
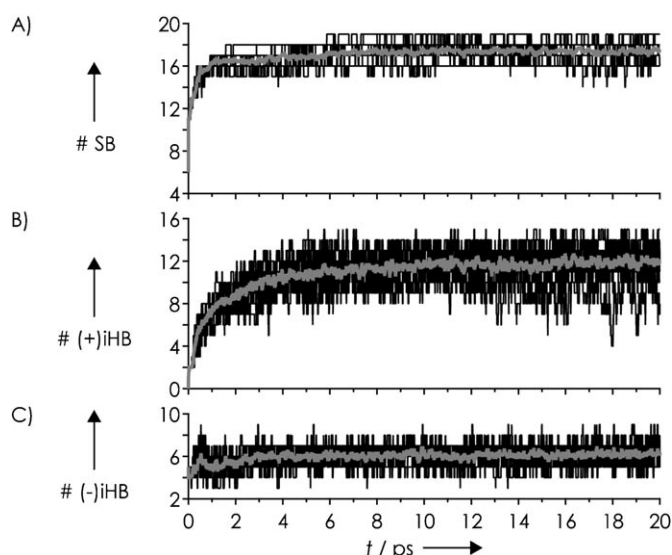
Figure 3. Number of: A) salt bridges (SB), B) ionic hydrogen bonds involving protonated side chains ((+)iHB), and C) ionic hydrogen bonds involving deprotonated side chains ((−)iHB) for ten trajectories (black lines) versus simulation time; average values shown as thick gray lines.

Effect of initial charge distribution

Next we asked whether the new side-chain interactions formed randomly, or if side-chain reorientation was affected by the overall distribution of charges. Native equine (Fe^{III})–cytochrome c has a relatively large electric dipole moment of 1.08×10^{-27} C m, mainly as a result of the inhomogeneous distribution of negatively charged residues on the protein surface.[12] However, calculation of electric dipole moments is rather complex for proteins,[13] and our primary interest was in the distribution of charges. We therefore introduced a Z vector that originates from the geometrical center of all negative charges, and points to the center of all positive charges. Its length is a direct measure of the protein's charge asymmetry (Figures 4A, B). The Z-vector orientation was calculated with respect to a plane spanned by three of the heme's nitrogen atoms, and described by two angles, Φ and Ψ (see Computational Methods for details).

The Z-vector length decreased exponentially with simulation time from 4.61 Å for the native structure to an average value of 3.07 Å after 10 ps, whereas its orientation did not change significantly (Figures 4C–E). The rate constant for the decrease in vector length was $(1.027 \pm 0.008) \times 10^{12}$ s^{-1}, which is about halfway between those for SB and iHB formation. This indicates that all newly formed electrostatic interactions contribute to the rapid decrease of Z-vector length. Apparently, reorientation of all charged side chains is governed by the initial charge distribution and proceeds in such a way as to minimize the protein's charge asymmetry and therefore its dipole moment in the gas phase.

Changes in RMSD

In addition to the ten short (0–20 ps) and highly-resolved trajectories discussed above, we also performed MD simulations
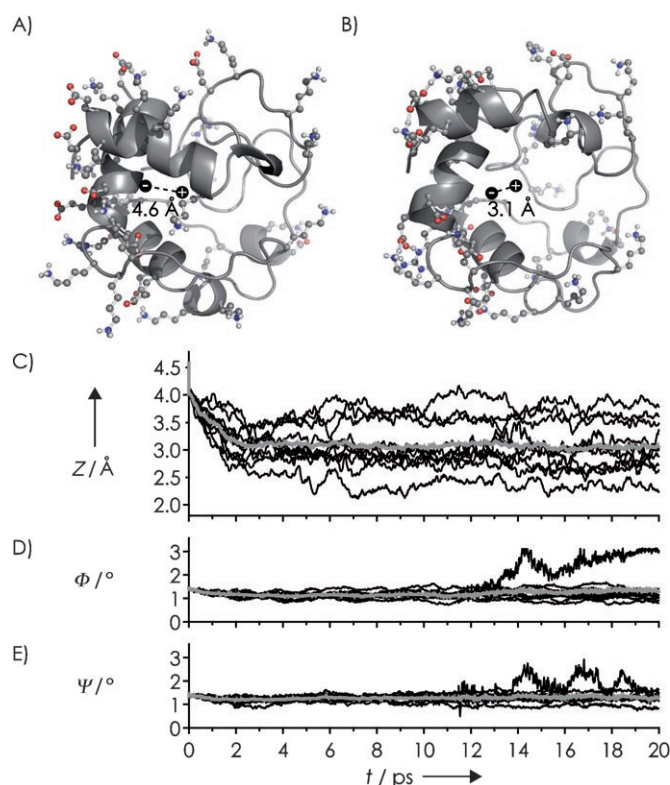
Figure 4. Distance between positive and negative charge centers for: A) NMR structure 1AKK, and B) representative MD structure after 2.716 ps simulation time; charged residues are shown as balls and sticks. C) Length of Z vector, and angles D) Φ and E) Ψ of Z-vector orientation for ten trajectories (black lines) versus simulation time; average values are shown as thick gray lines.

with moderate time resolution and simulation times of up to 4.2 ns. Visual inspection of MD structures from these simulations showed no new structural features other than those already found in the short simulations. Figure 5 shows root mean square deviations (RMSD) from the starting PDB struc-
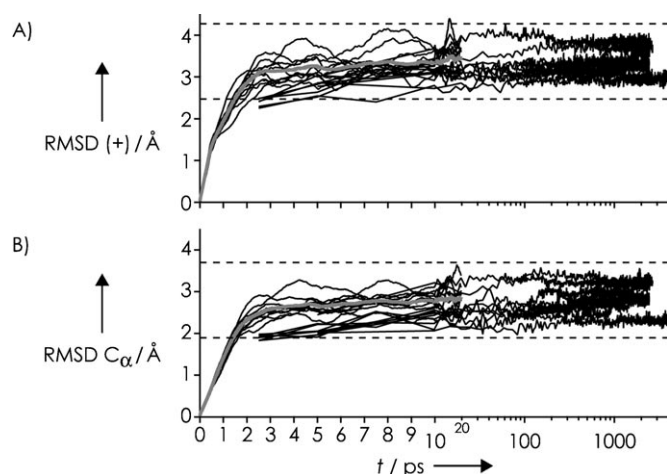
Figure 5. Root mean square deviation (RMSD) from NMR structure 1AKK for all trajectories (black solid lines) of: A) positively charged residues, and B) Cα atoms for simulation times of up to 4.7 ns. Thick gray lines are average values for the short (0–20 ps) MD simulations.

ture 1AKK for positively charged basic residues and C$_\alpha$ atoms for all trajectories. The average RMSD of positively charged residues for the short trajectories increases exponentially with a rate constant of $(0.860 \pm 0.003) \times 10^{12}$ s^{-1}, which is between the rate constants for SB and (+)iHB formation. After about 10 ps, the RMDS reached a plateau at 3.4 Å. Data from the longer trajectories all lie in the range (3.4 ± 0.9) Å for simulation times > 10 ps (dashed lines in Figure 5 A).

Similar results were found for the C$_\alpha$ atoms, for which the average RMSD increased with a slightly smaller rate constant of $(0.826 \pm 0.002) \times 10^{12}$ s^{-1}. The plateau value for simulation times > 10 ps was also smaller (2.8 Å); this is consistent with substantial reorientation of the charged residues while largely preserving the native backbone fold. The C$_\alpha$ RMSD values from the longer trajectories all lie in the range (2.8 ± 0.9) Å for simulation times > 10 ps (dashed lines in Figure 5 B). The plateaus found for both side-chain and C$_\alpha$ RMSD values from all simulations suggest that after a short phase (~ 10 ps) of side-chain reorientation, intermediate gas phase structures stabilized by new electrostatic interactions are formed in ESI.
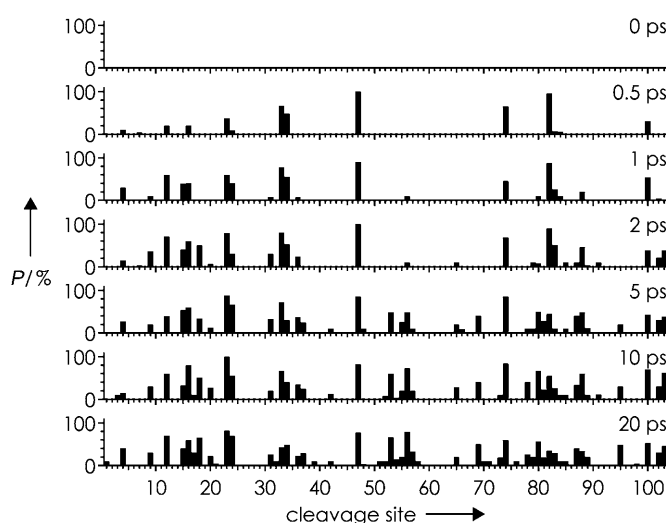
Comparison with NECD data

NECD has recently provided residue-specific information on the structural changes of native equine cytochrome c following transfer into the gas phase.[9b] The NECD data revealed a sequential unfolding mechanism, with the terminal helices and the Ω loop unfolding first (Figure 1 A); in solution, the terminal helices are the last to unfold.[14] In the proposed NECD mechanism,[9a] backbone cleavage of gaseous cytochrome c ions occurs when: 1) a proton is in close proximity to the cleavage site and 2) residues next to the cleavage site are in contact with the protein's heme group, which is thought to transfer an electron. In native equine (Fe^{III})–cytochrome c,[5] 26 out of 104 residues are in noncovalent contact with the heme. These noncovalent contacts include hydrophobic interactions of 17 residues, hydrogen bonding with the heme propionates of four residues, coordinative bonding with the heme iron of H18 and M80, and unspecific interactions with the heme of T40, A43, and Y48. According to the proposed mechanism,[9a] NECD cleavage can occur next to any of these residues, provided that contact with the heme is retained on transfer into the gas phase and a nearby positive charge is available. Whereas in the native structure all positively charged residues point away from the protein surface and potential cleavage sites, positive charge can become available for NECD through the formation of iHBs involving positively charged side chains and amide oxygens (Figure 2 B) or nitrogens.

However, the electron-transfer step proposed for covalent bond dissociation in NECD cannot be reproduced by *standard* MD simulations. Nevertheless, we can connect experimental NECD data with our MD results by analyzing the latter for the proposed requirements for backbone cleavage (see points (1) and (2) above). For this purpose, we introduced two parameters, the "proton score" (P) and the "heme score" (H). For calculation of P as a measure of how frequently a proton is in proximity to a given cleavage site, the distances between all

charge-carrying nitrogen atoms of lysine or arginine residues and the backbone amide oxygen or nitrogen were measured. The fraction of cases for which any of these distances was less than 3 Å gave the site-specific proton score.

The *H* value is a measure of how frequently the residues that frame a given cleavage site are in close proximity to the heme. As each backbone cleavage site is framed by two amino acids, distances between each atom of these two amino acids and each atom in the heme group were calculated. The fraction of cases for which any of these distances was less than 5 Å gave the site-specific heme score. Score analysis was performed separately for all backbone sites in the protein.
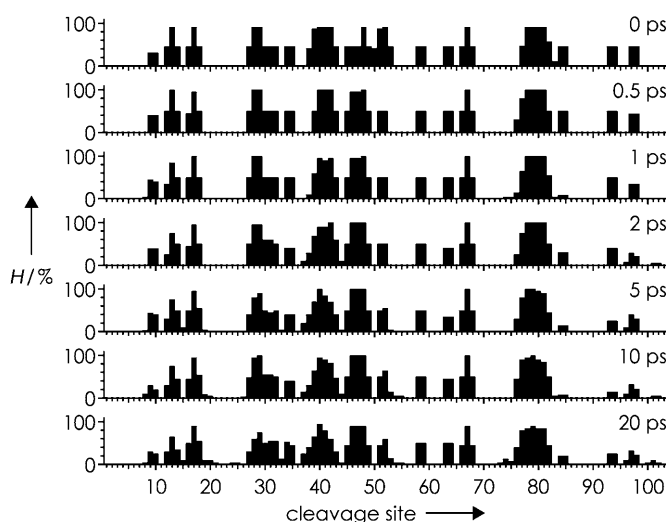
Figure 6 shows site-specific proton scores for simulation times 0–20 ps. The *P* value for the native structure (0 ps) was zero for all sites, as all charged residues are exposed to solvent and point away from the protein surface (Figures 1 B and 4 A).

Figure 7. Site-specific heme score (*H*) versus cleavage site for simulation times 0, 0.5, 1, 2, 5, 10, and 20 ps.

The calculated site-specific *P*, *H*, and NECD scores from this analysis are shown in Figures 8 A–C. Linear least square fitting of calculated versus experimental (Figure 8 D) data gave residuals with standard deviations of 36, 24, and 13 for the heme, proton, and NECD scores, respectively. Neither the heme nor the proton score alone showed particularly good agreement with experimental data, whereas a much better correlation (improved by factors of 2.8 and 1.9) is found for the NECD score. This includes cleavage after residue 12 (cleavage site 12), six

Figure 6. Site-specific proton score (*P*) versus cleavage site for simulation times 0, 0.5, 1, 2, 5, 10, and 20 ps.
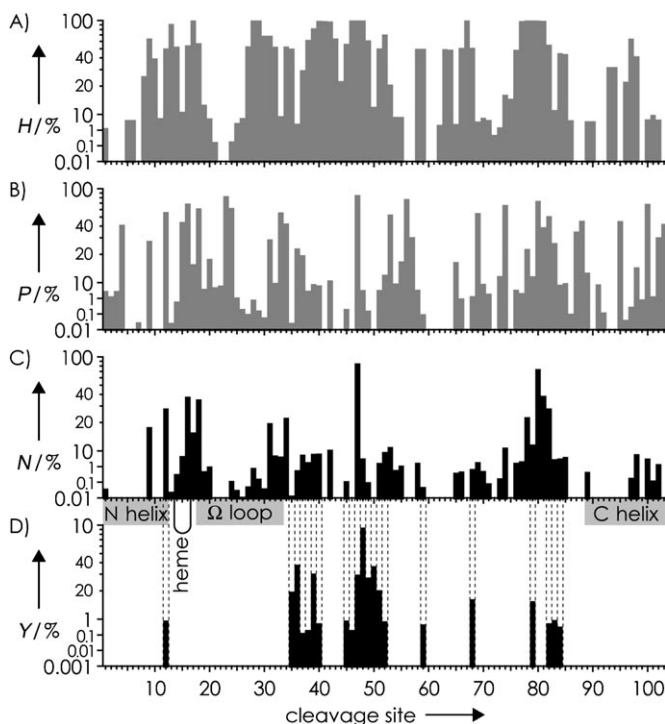
The proton score increased rapidly with increasing simulation times as a consequence of (+)iHB formation. Consistent with the plateau in the number of (+)iHBs for simulation times of >10 ps (Figure 3 B), the proton scores at 10 and 20 ps were very similar. The site-specific heme score, on the other hand, did not change significantly for simulation times of up to 20 ps (Figure 7); this is consistent with preservation of the backbone fold throughout the simulations.

To include both hypotheses 1) and 2) from the proposed mechanism in our model for prediction of NECD cleavages, we multiplied the proton and heme scores to obtain predicted site-specific NECD yields. Multiplication of the scores tests if both must be high for efficient cleavage under the assumption that both are independent. For increased accuracy in our computational prediction, we combined data for which C_α RMSD values were in the range (2.8 ± 0.9) Å; that is, all frames from the short trajectories for simulation times >10 ps and data from the long trajectories of up to 4.2 ns were combined.

Figure 8. Site-specific A) heme score (*H*), B) proton score (*P*), and C) NECD score (*N*) predicted from MD data, and D) experimental NECD yield (*Y*, in % of all ions detected) from ref. [9b].

adjacent cleavages at sites 35–40, five cleavages at sites 45–49, two cleavages at sites 51 and 52, cleavage at sites 59, 68, 79, and three cleavages at sites 82–84. However, computation also predicts NECD products from cleavage of the N-terminal helix, the Ω loop, and the C-terminal helix regions (Figure 8C) that were not observed experimentally (Figure 8D).

The absence of these products and the disappearance of additional predicted products at higher inlet capillary temperatures in the NECD experiment is consistent with partial unfolding of native cytochrome c in our 0.5 mm i.d. inlet capillary[9] such that the corresponding residues no longer have contact with the heme when NECD occurs (zero heme score). A 0.6 ms residence time has been estimated for a 0.4 mm inlet capillary.[15] From our earlier calculations,[8] evaporation of the final hydration shell results in a significant decrease in protein ion temperature, and ion heating (e.g., in the heated capillary) is necessary for full desolvation. This suggests that the unfolding leading to NECD has a temperature-dependent timescale in the low millisecond range, and shows that the native structure has been little modified by reorientation of the charged side chains on a low picosecond timescale.

Conclusions

The MD simulations reported here reveal that the very first structural changes after desolvation of native cytochrome c generally involve charged side chains. Rather than the breakage of noncovalent bonds, we analyzed the rapid formation of SBs and iHBs on the protein surface. These new interactions did not form randomly, but occurred in a way that significantly reduced the protein's dipole moment. In this transient MD structure, the sites of closest approach between side-chain N^+—H and backbone heteroatoms, and the intramolecular contacts with the heme, agree well with the cleavage sites of the NECD spectrum. This confirms the postulated NECD mechanism and indicates that the backbone fold remains essentially the same as that in solution, until heating beyond the energy required for complete desolvation induces unfolding on a milliseconds timescale. Apparently, any global structural changes caused by desolvation are preceded by rearrangements of charged side chains, and result in transiently stabilized structures with a backbone fold that is essentially the same as that in solution. Because exposed charged side chains are a common feature of globular proteins, and the rapid formation of SBs and iHBs on the protein surface observed here has no specific structural requirements, we anticipate similar behavior after desolvation for all other globular proteins. These newly formed electrostatic interactions could be responsible for transient stabilization of native folds after removal of bulk water, and make it possible to detect increasingly large and complex biomolecular architectures by mass spectroscopy.[1,2] On the other hand, arresting the formation of electrostatic interactions after desolvation by heating and/or solution additives allows for "top-down" characterization of proteins as large as 200 kDa.[16]

Computational Methods

Atomistic detail Molecular Dynamics[17] simulations were performed with MOIL,[18] a modeling package for simulations of biological molecules. The MOIL force field is based on AMBER[19] and OPLS[20] force fields. The potential used in this work was tuned to polar condensed phase simulations. However, since proteins are large molecules, we expect them to act as their own heat baths and recover some condensed phase properties. Successful simulations of proteins in nonpolar environments (such as membranes) further support the application of this type of force field for the problem at hand. No cut-off distance for nonbonded interactions was used in any of the simulations. Also, no SHAKE algorithm was used to ensure that all degrees of freedom were included in the calculations.

All simulations were carried out under constant energy conditions in vacuo (no solvent water), with the NMR structure of native equine (Fe^{III})–cytochrome c (PDB ID: 1AKK)[5] as starting structure. To match conditions in NECD experiments (pH 5 of ESI solution), charge sites were assigned according to calculated pK_a values of ionizable residues in native equine (Fe^{III})–cytochrome c (for details see ref. [10]). Briefly, all aspartic and glutamic acid residues, both heme propionates, and the C terminus are deprotonated, all lysine and arginine residues were protonated, and histidine residues were uncharged; this resulted in a net charge of +7 for (Fe^{III})–cytochrome c. This value corresponds closely with reported average net charge values ($\sim +8$) for ESI of aqueous (Fe^{III})–cytochrome c solutions at pH 5.[21] Because the location of charges after ESI is not known, we used the solution charge distribution for the MD calculations.

Two sets of MD simulations were carried out. For the first set, the starting structure 1AKK was assigned ten different initial atom velocity distributions, each of which represents a Boltzmann distribution at 300 K. The ten resulting trajectories had time-steps of 0.2 fs and a total length of 20 ps. Frames were saved every 20 steps; this resulted in a frame every 4 fs. We refer to this first set of simulations as the short and highly resolved simulations. For the second set of simulations, a short (0.5 ps) MD simulation of the starting structure 1AKK was performed at 30 K to sample slightly different initial structures (all-atom RMSD < 0.9 Å compared to 1AKK) for the dynamics. Structures extracted from this trajectory were used as initial structures to generate ten trajectories with a starting temperature of 300 K; the simulations were run with time-steps of 0.25 or 0.5 fs. Frames were saved every 10000 steps; this resulted in frames every 2.5 or 5 ps. The total lengths of the simulations in the second set varied between 350 ps and 4.2 ns. We refer to this second set of simulations as the longer simulations with moderate time resolution. The time-steps used in all our MD simulations are smaller than the 1 fs step typically used for proteins, but were necessary to maintain a high level of energy conservation.

For the identification of SBs, we measured the distances between all nitrogens of lysine and arginine side chains that carried a positive charge, and all oxygens of glutamic and aspartic acid that carried a negative charge. A SB[22] between two residues of opposite charge was defined when the distance between positive and negative charges was smaller than 3 Å. For identification of (+)iHBs, we measured the distances between all nitrogens of lysine and arginine side chains that carried a positive charge and all backbone amide oxygen or nitrogen atoms. A (+)iHB was defined between a positively charged side chain and the backbone when the distance between charged nitrogen and backbone heteroatom was smaller than 3 Å; this value was chosen based on typical heteroatom dis-

tances for (+)iHBs in smaller systems.[23] For identification of (−)iHBs, we measured the distances between all oxygens of glutamic and aspartic acid side chains that carried a negative charge and all backbone amide oxygen or nitrogen atoms. A (−)iHB was defined between a negatively charged side chain and the backbone when the distance between charged oxygen and backbone heteroatom was smaller than 3 Å; O⋯N and O⋯O distances for (−)iHBs that involved the heme propionates in native (Fe^{III})–cytochrome c were between 2.65 and 2.80 Å.

The geometrical centers of positive and negative charges were calculated as follows. For the positive charge center, individual charge vectors, $\vec{r}_p$, that originated from an arbitrary reference point and pointed to the positive charges, were multiplied by the corresponding charge values q_p. The vectorial sum of the resulting vectors was divided by the total number of positive charges to give a vector that pointed to the center of positive charges. The vector that pointed to the center of negative charges was calculated in the same manner. Subtraction of the vector that pointed to the center of negative charges from the vector pointing to the center of positive charges gave the vector $\vec{z}$ [Eq. (1)], the length (in Å) and orientation of which is independent of the reference point chosen.

$$\vec{Z} = \frac{\sum_p \vec{r}_p \cdot q_p}{\sum_p q_p} - \frac{\sum_n \vec{r}_n \cdot q_n}{\sum_n q_n} \tag{1}$$

For specification of Z-vector orientation, two angles, Φ and Ψ, were defined with respect to the plane spanned by three out of the four heme nitrogen atoms (the distance between the fourth nitrogen atom and this plane was very small throughout all simulation, about 0.1 Å on average, so that our reference plane was essentially the heme plane). Here Φ is the angle between $\vec{z}$ and its orthogonal projection onto the plane, and Ψ is the rotation angle of $\vec{z}$ around a vector perpendicular to the plane.

For calculation of site-specific proton scores, distances between all charge-carrying nitrogen atoms of lysine or arginine residues and the backbone amide oxygen or nitrogen associated with a given cleavage site were measured for each frame. When any of these distances was less than 3 Å (i.e., when an (+)iHB was found), a score of one was assigned to the cleavage site. Otherwise a score of zero was assigned. Proton scores of all frames considered were added, divided by the number of frames, and multiplied by 100 to give percent values. Site-specific heme scores were calculated in a similar way, except that the cut-off distance for protein–heme contacts was 5 Å (this was necessary because MOIL treats CH$_3$ groups as single atoms) and that individual score values were 0.5 and 0 instead of 1 and 0 (this accounts for the fact that each cleavage site is framed by two amino acids, each of which can be in contact with the heme). For evaluation of the 5 Å cut-off distance, we compared the 26 noncovalent protein/heme contacts (<3 Å) found by manual examination of the 1AKK structure (using the molecular visualization program RasMac_PPC) with the noncovalent protein–heme contacts of the same structure found with MOIL for different cut-off values. A cut-off value of 4 Å was insufficient and reproduced only 22 out of the 26 protein–heme contacts, whereas a cut-off value of 5 Å reproduced all manual assignments. For increased statistical accuracy in Figures 6 and 7, scores were calculated from eleven frames from each trajectory and the time indicated (frame at the time indicated, plus the five preceding and five subsequent frames, covering time intervals of 40 fs; the 0 ps calculation used the 1AKK structure and ten subsequent frames); this re-

sulted in 110 frames for each time indicated. For calculation of score values in Figure 8, 25 010 frames from the short simulations (time-range 10–20 ps) and 8308 frames from the longer simulations were used.

Keywords: desolvation · electrospray ionization · molecular dynamics · native electron capture dissociation · protein structures

[1] a) J. A. Loo, *Mass Spectrom. Rev.* **1997**, *16*, 1–23; b) A. J. R. Heck, R. H. H. van den Heuvel, *Mass Spectrom. Rev.* **2004**, *23*, 368–389; c) B. T. Ruotolo, C. V. Robinson, *Curr. Opin. Chem. Biol.* **2006**, *10*, 402–408.

[2] a) P. D. Schnier, J. S. Klassen, E. F. Strittmatter, E. R. Williams, *J. Am. Chem. Soc.* **1998**, *120*, 9605–9613; b) V. Gabelica, E. D. Pauw, *J. Mass Spectrom.* **2001**, *36*, 397–402; c) V. Gabelica, E. S. Baker, M. P. Teulade-Fichou, E. De Pauw, M. T. Bowers, *J. Am. Chem. Soc.* **2007**, *129*, 895–904.

[3] J. B. Fenn, M. Mann, C. K. Meng, S. F. Wong, C. M. Whitehouse, *Science* **1989**, *246*, 64–71.

[4] K. Breuker in *Principles of Mass Spectrometry Applied to Biomolecules* (Eds.: J. Laskin, C. Lifshitz), Wiley, New York, **2006**, pp. 177–212.

[5] L. Banci, I. Bertini, H. B. Gray, C. Luchinat, T. Reddig, A. Rosato, P. Turano, *Biochemistry* **1997**, *36*, 9867–9877.

[6] a) M. Dole, L. L. Mack, R. L. Hines, R. C. Mobley, L. D. Ferguson, M. B. Alice, *J. Chem. Phys.* **1968**, *49*, 2240–2249; b) G. Schmelzeisen-Redeker, L. Bütfering, F. W. Röllgen, *Int. J. Mass Spectrom. Ion Processes* **1989**, *90*, 139–150.

[7] a) J. Fernandez de la Mora, *Anal. Chim. Acta* **2000**, *406*, 93–104; b) M. Peschke, A. Blades, P. Kebarle, *J. Am. Chem. Soc.* **2002**, *124*, 11519–11530; c) N. Felitsyn, M. Peschke, P. Kebarle, *Int. J. Mass Spectrom.* **2002**, *219*, 39–62; d) A. T. Iavarone, E. R. Williams, *J. Am. Chem. Soc.* **2003**, *125*, 2319–2327; e) U. H. Verkerk, M. Peschke, P. Kebarle, *J. Mass Spectrom.* **2003**, *38*, 618–631; f) V. J. Nesatyy, M. J. F. Suter, *J. Mass Spectrom.* **2004**, *39*, 93–97; g) P. Pan, H. P. Gunawardena, Y. Xia, S. A. McLuckey, *Anal. Chem.* **2004**, *76*, 1165–1174; h) A. J. R. Heck, R. H. H. van den Heuvel, *Mass Spectrom. Rev.* **2004**, *23*, 368–389; i) U. H. Verkerk, P. Kebarle, *J. Am. Soc. Mass Spectrom.* **2005**, *16*, 1325–1341; j) I. A. Kaltashov, A. Mohimen, *Anal. Chem.* **2005**, *77*, 5370–5379.

[8] M. Z. Steinberg, K. Breuker, R. Elber, R. B. Gerber, *Phys. Chem. Chem. Phys.* **2007**, *9*, 4690–4697.

[9] a) K. Breuker, F. W. McLafferty, *Angew. Chem.* **2003**, *115*, 5048–5052; *Angew. Chem. Int. Ed.* **2003**, *42*, 4900–4904; b) K. Breuker, F. W. McLafferty, *Angew. Chem.* **2005**, *117*, 4989–4992; *Angew. Chem. Int. Ed.* **2005**, *44*, 4911–4914.

[10] K. Breuker, *Int. J. Mass Spectrom.* **2006**, *253*, 249–255.

[11] J. M. Daniel, S. D. Friess, S. Rajagopalan, S. Wendt, R. Zenobi, *Int. J. Mass Spectrom.* **2002**, *216*, 1–27.

[12] a) W. H. Koppenol, E. Margoliash, *J. Biol. Chem.* **1982**, *257*, 4426–4437; b) W. H. Koppenol, J. D. Rush, J. D. Mills, E. Margoliash, *Mol. Biol. Evol.* **1991**, *8*, 545–558.

[13] S. Takashima, *Biophys. J.* **1993**, *64*, 1550–1558.

[14] a) M. M. G. Krishna, Y. Lin, J. N. Rumbley, S. W. Englander, *J. Mol. Biol.* **2003**, *331*, 29–36; b) H. Maity, M. Maity, S. W. Englander, *J. Mol. Biol.* **2004**, *343*, 223–233.

[15] U. A. Mirza, B. T. Chait, *Int. J. Mass Spectrom. Ion Processes* **1997**, *162*, 173–181.

[16] X. Han, M. Jin, K. Breuker, F. W. McLafferty, *Science* **2006**, *314*, 109–112.

[17] J. A. McCammon, B. R. Gelin, M. Karplus, *Nature* **1977**, *267*, 585–590.

[18] R. Elber, A. Roitberg, C. Simmerling, R. Goldstein, H. Li, G. Verkhivker, C. Keasar, J. Zhang, A. Ulitsky, *Comput. Phys. Commun.* **1995**, *91*, 159–189.

[19] S. J. Weiner, P. A. Kollman, D. A. Case, U. C. Singh, C. Ghio, G. Alagona, S. Profeta, P. Weiner, *J. Am. Chem. Soc.* **1984**, *106*, 765–784.

[20] W. L. Jorgensen, J. Tirado-Rives, *J. Am. Chem. Soc.* **1988**, *110*, 1657–1666.

[21] a) L. Konermann, D. J. Douglas, *Biochemistry* **1997**, *36*, 12296–12302; b) L. Konermann, D. J. Douglas, *Rapid Commun. Mass Spectrom.* **1998**, *12*, 435–442.

[22] S. Kumar, R. Nussinov, *ChemBioChem* **2002**, *3*, 604–617.

[23] M. Meot-Ner, *Chem. Rev.* **2005**, *105*, 213–284.